We are IntechOpen,
the world's leading publisher of
Open Access books
Built by scientists, for scientists

4,800
Open access books available

122,000
International authors and editors

135M
Downloads

Our authors are among the

154
Countries delivered to

TOP 1%
most cited scientists

12.2%
Contributors from top 500 universities

WEB OF SCIENCE™

Selection of our books indexed in the Book Citation Index
in Web of Science™ Core Collection (BKCI)

Interested in publishing with us?
Contact book.department@intechopen.com

Numbers displayed above are based on latest data collected.
For more information visit www.intechopen.com

Elastomeric Electronics: A Microfluidic Approach

Shi Cheng

Additional information is available at the end of the chapter

http://dx.doi.org/10.5772/50208

1. Introduction

Thousands of millions of electronic units have been produced since the first invention of electronics. These devices and systems, in which stiff, solid metals, insulators, and semiconductors have dominated for ages, are exclusively made in the rigid format, and usually retain a static shape once fabricated. Things have however changed recently. Researchers are currently attempting to shape a soft and rubbery future for electronics, where elastic materials like elastomers would be widely used to replace conventional rigid materials. The reason is rather simple. We as human beings are soft, just like most other living creatures in nature, but existing electronics are not. Shouldn't we create some kind of new electronics that resemble ourselves?

Extensive research activities on developing elastomeric electronics that may withstand severe bending, twisting, and straining, with maintained electronic functions, have been recently carried out. The mechanical characteristics of gold thin films on polydimethylsiloxane (PDMS) surfaces: wrinkles and cracks, have been investigated by Whitesides and Hutchinson for the first time in 1998 [1]. Subsequently, wrinkled electrodes on pre-stretched elastic substrates were employed to implement electroactive polymer actuators [2], and studies on wrinkled gold electrodes on PDMS substrates were conducted in the Wagner's and Suo's groups at Princeton [3],[4]. Micromechanics and manufacturing processes based on relaxed and pre-stressed PDMS slabs were developed in-depth. The most significant contributions were made by the Rogers's group at University of Illinois, Urbana-Champaign, where stretchable and foldable silicon integrated circuits (ICs) on "wavy" silicon ribbons (from Silicon On Insulator (SOI)) in PDMS were proposed for fully integrated stretchable electronics [5],[6]. Dozens of appealing devices based on stretchable silicon ICs, including electronic eye sensor [7], smart gloves/skins [8], implanted medical devices [9], and wearable ergonomic biomedical sensors [10], have been demonstrated. An alternative approach utilizing anisotropic etching of bulk wafers was also introduced [11],[12]. Later, thin meandered stretchable interconnects encased in silicone rubber substrates, operating at

different frequencies, were presented [13]-[15]. New electrical nanocomposite materials containing sliver nano-particles or carbon nanotubes/graphene that can flex and strain showed promising results as well [16],[17].

Microfluidics based stretchable electronics were initiated by Whitesides, who first studied low temperature metling solder filled microstructured elastomeric channels [18],[19]. Recently, this concept was extended to implement elastic direct current (DC) circuits, by incorporating eutectic gallium and indium alloy (EGaIn) into microfluidic channels in thin sheets of elastomers [20]-[22]. However, all these previously mentioned studies deal with either low-frequency ICs or relatively simple interconnects. Stretchable electronics at radio frequencies remained an unexploited field until early 2009, at which time Cheng demonstrated the first stretchable fluidic antennas, for enabling wireless communication and remote sensing [23],[24]. Similar work was reported afterwards using EGaIn alloy as conductors for the antennas instead of Galinstan [25]. Significantly enhanced elasticity of the resulting antennas could be achieved by introducing a different type of siloxane [26], and mechanically reconfigurable antennas could also be realized [27]. In 2010, Cheng proposed a hybrid integration strategy for the first demonstration of active microfluidic stretchable RF electronics (μFSRFEs), an integrated RF radiation sensor, *cf*. Fig. 1.a. [28]. Cheng further developed the μFSRFEs to the multi-layer configurations, and reported an integrated stretchable large-area wireless strain sensor, as seen in Fig. 1.b. [29].
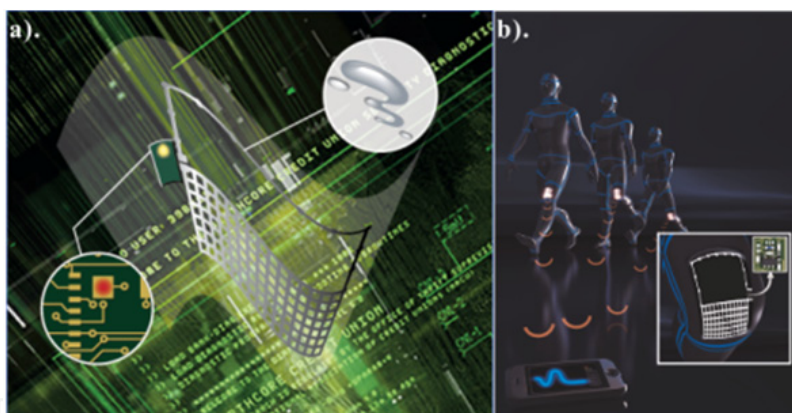

Figure 1. Foldable, flexible, stretchable elastomeric electronic devices: a). Microfluidic stretchable radiation sensor. b). Elastomeric, reversibly stretchable, large-area wireless strain sensor.

The following sections in this chapter address the recent progresses in the emerging field of microfluidics based elastomeric electronics. Fabrication processes, integration techniques, application examples, as well as future perspectives are presented and discussed.

2. Fabrication of single-layer microfluidics based passive elastomeric electronic devices

In brief, the manufacturing process steps can be summarized as follows: master construction, molding, liquid-alloy injection or filling, and encapsulation, *cf*. Fig. 2.
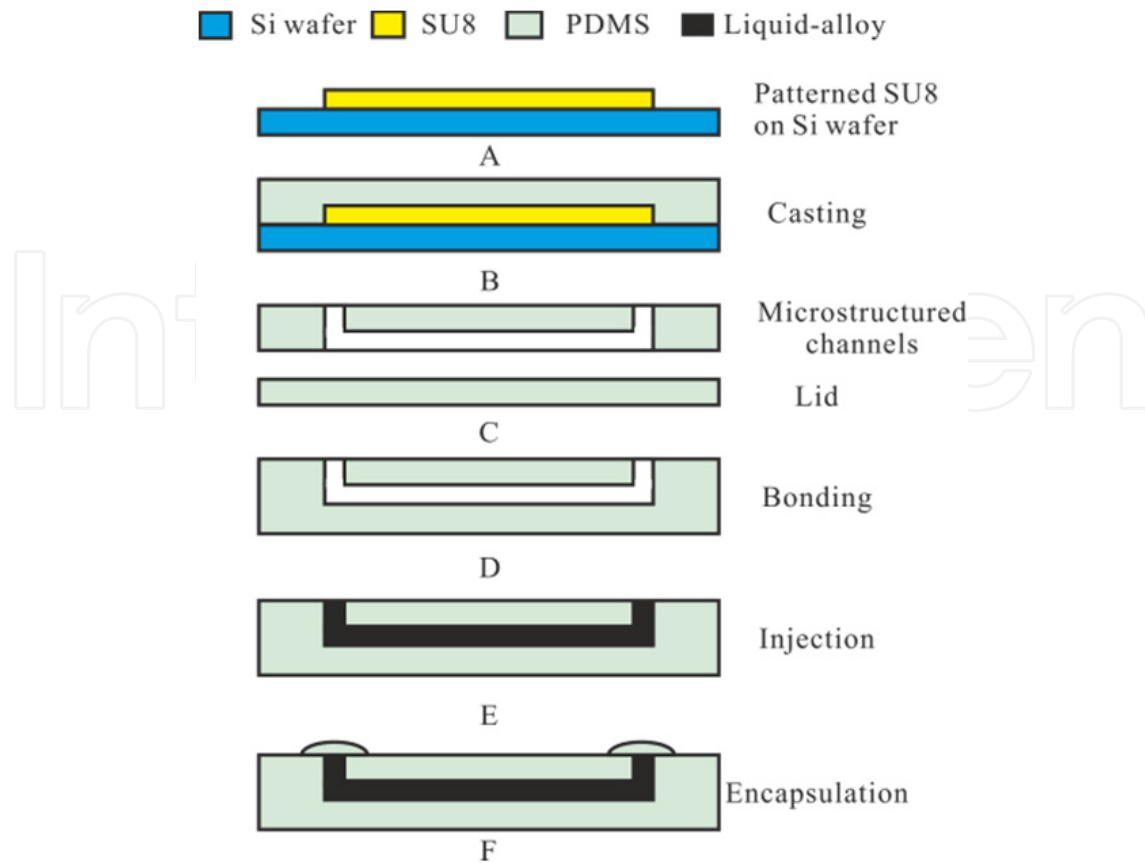
Figure 2. Manufacturing process steps of single-layer passive microfluidics based elastomeric electronics.

First of all, the design patterns are transferred to a 100 μm thick SU-8 100 (MicroChem, Newton, MA) layer on a silicon wafer with a standard soft lithography, and then developed and thermally stabilized at 150°C for 30 min to enhance the adhesion between SU-8 layer and silicon substrate. Subsequently, the PDMS prepolymer and cross linker (Elastosil RT601A and B, Wacker Chemie, Munich, Germany) are thoroughly mixed at a ratio of 9:1 (wt:wt) and poured onto the SU-8 master. After degassing, the PDMS mixture is cured at 70°C in an oven for 30 min. Then the cured thin PDMS replica is peeled off and a couple of holes are punched out for liquid alloy injection or filling. Meanwhile a thin blank PDMS lid is prepared using blank silicon wafer. Later, the PDMS replica and blank lid are bonded, using corona discharging (ETP, Chicago, IL, USA) activation. Through the punched holes in the PDMS, the liquid metal alloy (Galinstan, 68.5 % Ga, 21.5 % In, 10 % Sn, σ=3.46·106 S/m) is manually injected into the channels. This alloy remains in liquid state from -19°C to 1300°C. The ventilation outlets are encapsulated with uncured PDMS mixture as mentioned above.

3. Liquid metal, elastic, microfluidic unbalanced loop antenna

The fabrication process described in the previous section has been successfully employed to implement a single-layer, liquid metal, stretchable, unbalanced loop antenna, which consists of a radiating element and a semi-circular ground plane, as depicted in Fig. 3 [23]. Several cylindrical reservoirs are aligned along the upper tube of the antenna prototype to ensure

good electrical connections while being flexed. The presence of these reservoirs introduces slight resonance frequency decrease of the antenna. The lower semi-circular area acts as a ground plane for the antenna. A number of posts are aligned to space the top and bottom PDMS membranes in the ground area, which has negligible influence on the electrical characteristics of the antenna.
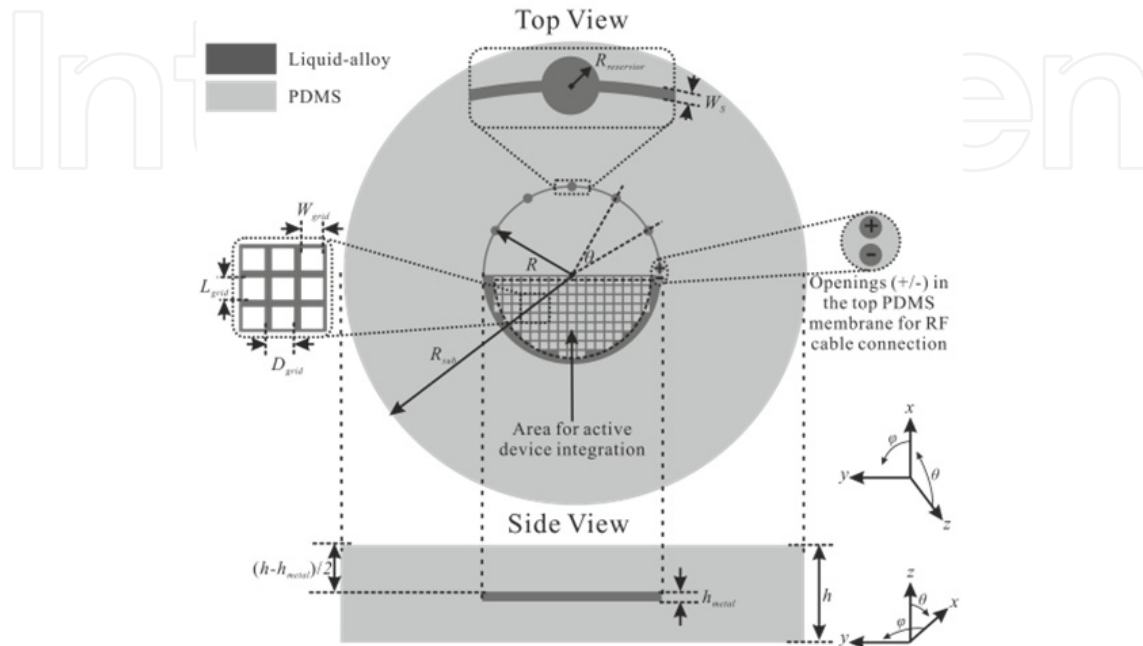

Figure 3. Geometrical schematic of stretchable unbalanced loop antenna: R=18.1 mm, R_{sub}=47.5 mm, $R_{reservior}$=1 mm, W_S=400 μm, L_{grid}=1.5 mm, W_{grid}=1.5 mm, D_{grid}=1.9 mm, h=1.0 mm, h_{metal}=100 μm, and θ=30°.

Mechanical properties of the antenna prototype were characterized experimentally. Fig. 4 shows that the resulting antenna is reversibly foldable, flexible, and stretchable. Severe bending and twisting in the tests did not cause any mechanical damages. In addition, the antenna can withstand extreme levels of strains of up to 40% along multiple axis. As a result of the uneven thickness of the PDMS substrate and the heterogeneous pattern of the antenna, slight mechanical inhomogeneity was observed while stressing along different orientations, *cf.* Figs. 4. b and c. In principle, elasticity of up to 100% should be in reach. Nevertheless, the openings in the membranes for electrical tests limit the mechanical deformability, reliability, and robustness, as the antenna can be easily torn from these openings.

Electrical properties of the antenna in its original state were obtained from numerical simulations. Experiments on port impedance and radiation characteristics of the antenna in both relaxed and flexed states were performed. Fig. 5 presents the simulated and measured reflection coefficients (S_{11}). The non-strained antenna features good impedance matching at 2.4 GHz, with an input impedance of approximately 75+15j Ω, Fig. 5.a. Applying strains on the antenna introduces an increase of the length of the upper radiating loop so that leads to a decrease on its resonance frequency, Fig. 5.b. In the case of stressing along *y*-axis, the antenna input resistance decreases due to the stronger coupling between the upper antenna arm and the lower ground plane, whereas this resistances goes up while stretching along *x*-axis.
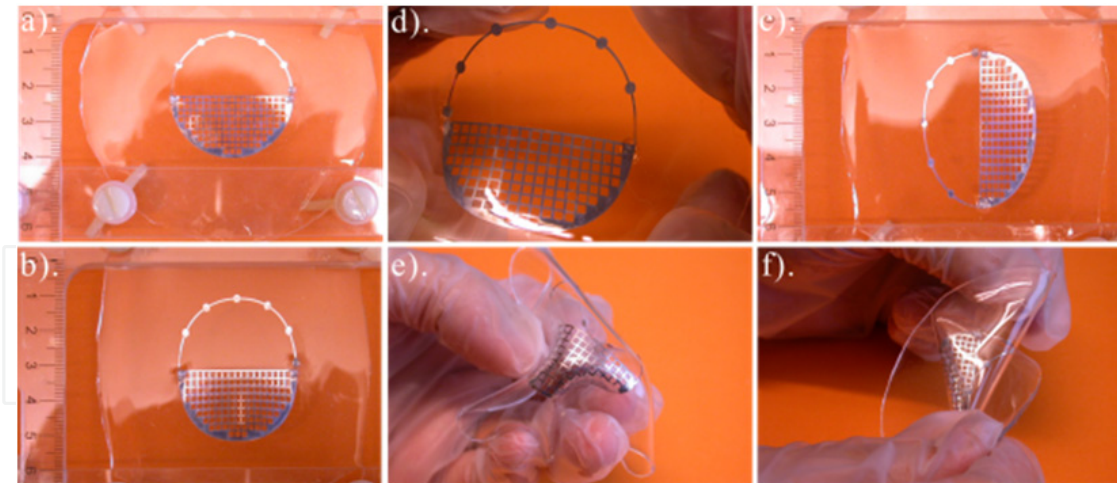
Figure 4. Photographs of the elastomeric fluidic unbalanced loop antenna: a). relaxed state, b). with 40% *x*-axis elongation, c). with 40% *y*-axis elongation, d). with biaxial elongation, e). bent state, and f). twisted state.
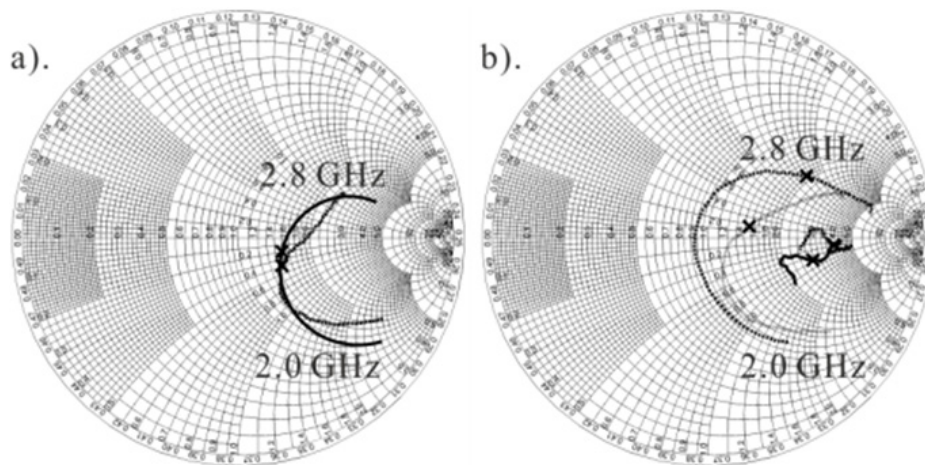

Figure 5. Simulated and measured port impedance of the elastic unbalanced loop antenna operating between 2.0 and 2.8 GHz: a). simulated (solid) and measured (dashed) S_{11} of the relaxed antenna; b). measured S_{11} of the flexed antenna with 20% *x*-axis (solid), 40% *x*-axis (dashed) and 20% *y*-axis (dotted), 40% *y*-axis (dashdot) elongation. The S_{11} at 2.4 GHz is marked by a cross sign on each curve.

Fig. 6 shows simulated and measured radiation patterns of the antenna prototype at 2.4 GHz.

As expected, the relaxed antenna resembles conventional unbalanced loops that exhibit broad beam coverage, especially in the *yz*-plane where nearly perfect omnidirectionality is seen. The maximum antenna gain is around 2.7 dBi, and the measured cross-polarization (G_ϕ in the *xz*-plane and G_θ in the *yz*-plane) is approximately 15 dB lower than the corresponding co-polarization. Variations of the radiation patterns of the strained antenna can be found, *cf*. Fig. 6.b. The omnidirectionality of the *yz*-plane radiation patterns degrades, particularly while the antenna is stressed along *y*-axis. The increasing cable influence caused by the *y*-axis strain explains the ripples within the angle of 45°-135° on the measured *xz*-plane radiation pattern. Also, the level of the measured cross-polarization of the stretched antenna slightly increases compared to that of the relaxed one.
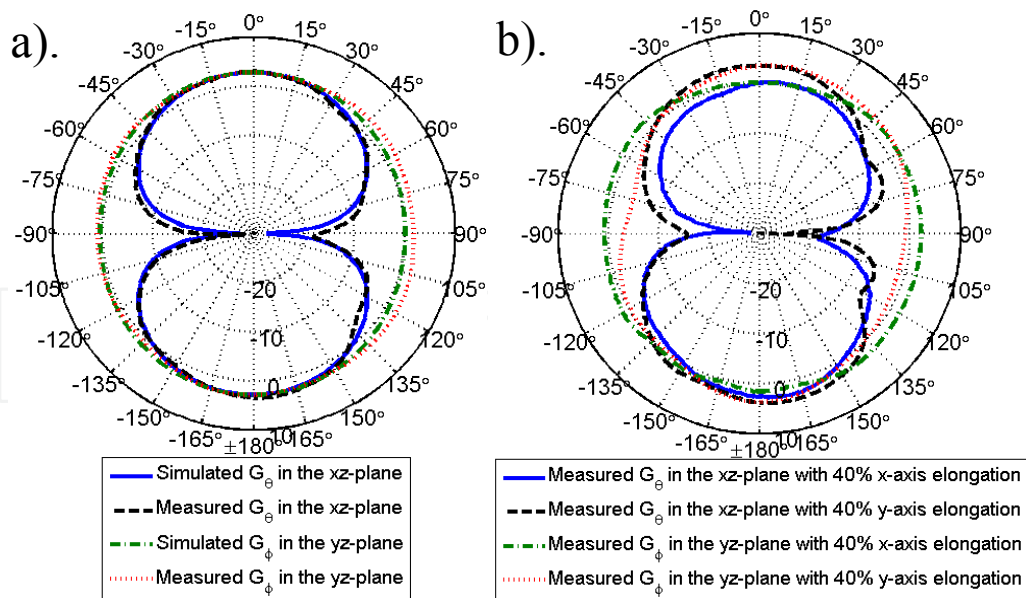
Figure 6. Simulated and measured radiation patterns of the a). relaxed and b). flexed antenna at 2.4 GHz. The corresponding coordinate system is depicted in Fig. 3. The antenna gain along ϕ and θ is defined as G_ϕ and G_θ, respectively.

High conductivity of Galinstan and large cross dimensions of the microfluidic channels attribute to low conductive losses and high radiation efficiency of the antenna. The measured data indicate a resonance frequency decrease of up to 18% while stretching, but the radiation efficiency at 2.4 GHz remains greater than 80%. In the experiments, no significant radiation efficiency decrease can be seen. This fact implies that galvanic connections in the microstructured elastomeric channels are not interrupted by straining. Good electrical continuity of the liquid alloy owes to its excellent wettability on PDMS substrate surfaces. Though the presented unbalanced loop antenna achieves good radiation properties, its resonance frequency detuning introduced by stretching leads to relatively poor total efficiency at 2.4 GHz. Other antenna concepts with more robust port impedance and radiation characteristics in response to deformation would be feasible alternative solutions.

4. Bendable, stretchable, fluidic UWB antenna

The concept of microfluidics based elastomeric electronics is then extended to realize a planar inverted cone antenna (PICA) for the ultrawideband (UWB) frequency range of 3.1-10.6 GHz [24]. The reason for choosing the PICA is that its impedance matching and radiation characteristics are expected to be insensitive to its mechanical deformation. Also, its uniplanar configuration makes it a suitable antenna type for a design that should be bendable and stretchable. Fig. 7 shows the design schematically, with a leaf-shaped radiation and a large ground plane.

Resembling to the previously demonstrated elastic unbalanced loop, the implemented PICA prototype features excellent reversible deformability in the mechanical tests, as shown in Fig. 8. Extreme levels of straining of up to 40% along either *x*- or *y*-axis do not cause any mechanical failures, *cf.* Figs. 8.b and d. Moreover, the resulting prototype also withstands

severe mechanical folding and twisting. After removal of applied mechanical forces, the antenna returns to its original state.
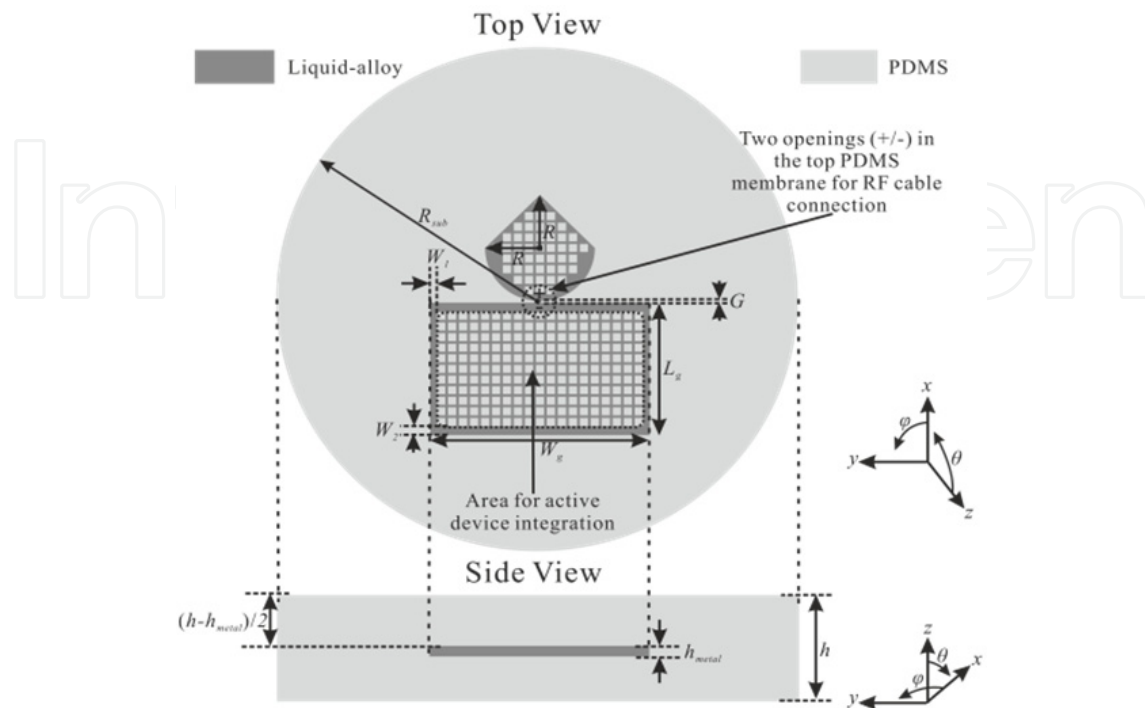

Figure 7. Geometry of the 2-D stretchable PICA. Dimensions are: R=10 mm, R_{sub}=47.5 mm, L_g=25 mm, W_g=40 mm, W_1=1.25 mm, W_2=1.75 mm, G=300 μm, h=1 mm, and h_{metal}=100 μm.
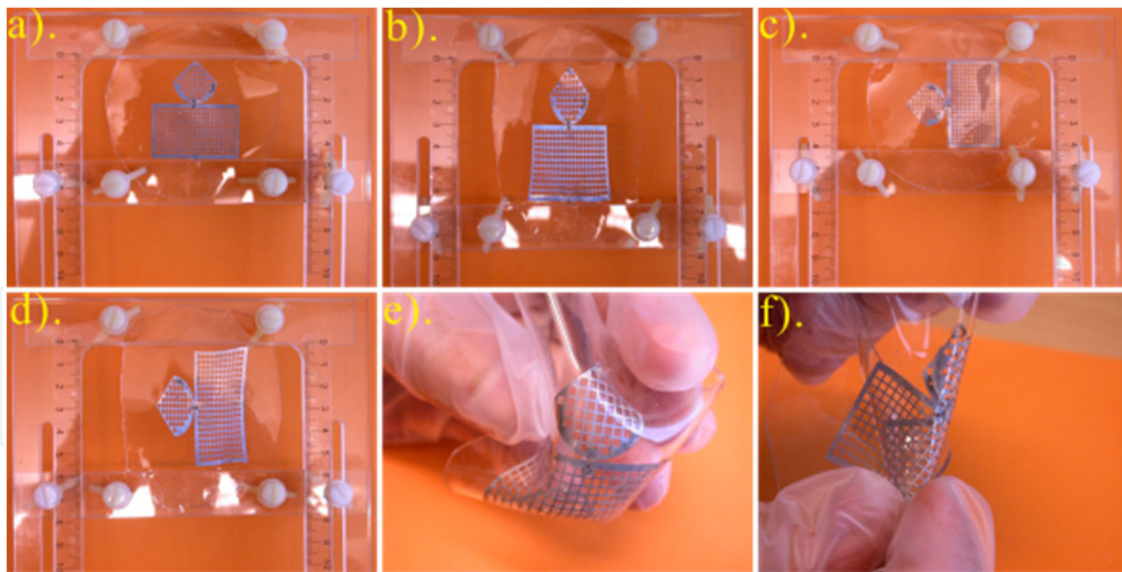

Figure 8. Photographs of the bendable, flexible, stretchable PICA: a). and c). relaxed state, b). strained antenna with 40% x-axis elongation, d). strained antenna with 40% y-axis elongation, e). folded antenna, and f). twisted antenna. The corresponding coordinate system is presented in Fig. 7.

Figs. 9 and 10 present simulated and measured reflection coefficients of the elastic, microfluidic PICA. The relaxed antenna shows good impedance match (S_{11} < -10 dB), within 3-11 GHz, both in numerical simulations and experiments.
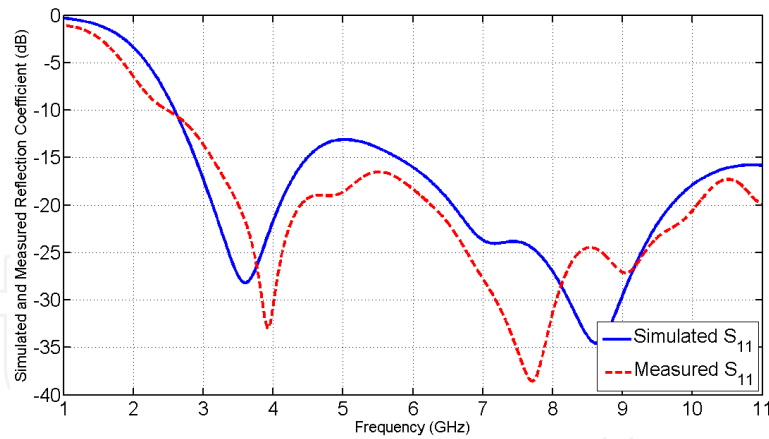
Figure 9. Simulated and measured S_{11} of the non-stretched antenna.

Applying strains along the *x*-axis results in the increased height of the antenna radiator so that its first resonance frequency decreases, *cf.* Fig. 10. Port impedance of the antenna is somewhat sensitive to its geometry, and consequently the antenna exhibits slightly varying impedance matching while stressed. However, good impedance match maintains at the entire UWB frequency band even if the antenna is strained to 40%.
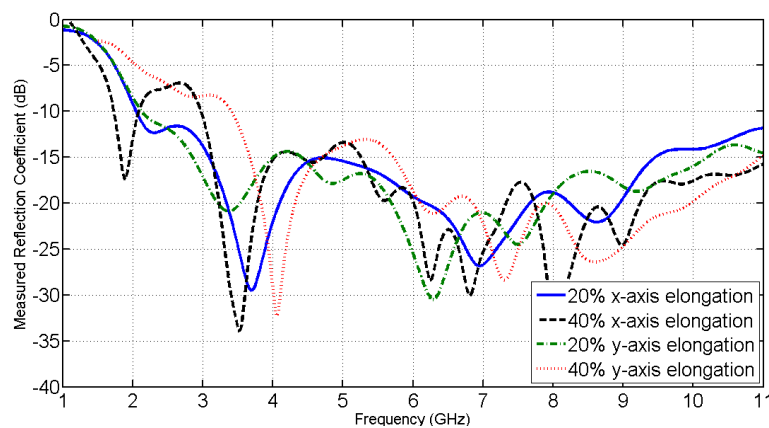

Figure 10. Measured reflection coefficients of the flexed antenna.

Measured radiation patterns at 2.5 GHz of the antenna in its relaxed and flexed states are displayed in Figs. 11 and 12. Similar to conventional fat monopole antennas, the non-strained antenna features broad coverage, especially in the *yz*-plane. The maximum antenna gain at 2.5 GHz was measured to be 2.2 dBi. The cross-polarization discrimination is very good. Numerical simulations are in line with the corresponding experimental data. Stretching the antenna along either *x*- or *y*-axis up to 40% introduces slight variations in the measured radiation patterns at 2.5 GHz, but without any significant gain reduction.

Similar simulations and experiments are also performed at 5 GHz, where ripples and slight asymmetry occur in the radiation patterns caused by disturbance from feed cable. The presence of higher order modes at 5 GHz together with the increasing cable influence degrades the cross-polarization discrimination. Compared to the experimental data at 2.5 GHz, larger variations on the measured radiation patterns at 5 GHz are observed while the antenna is in its strained states, particularly in the *yz*-plane.
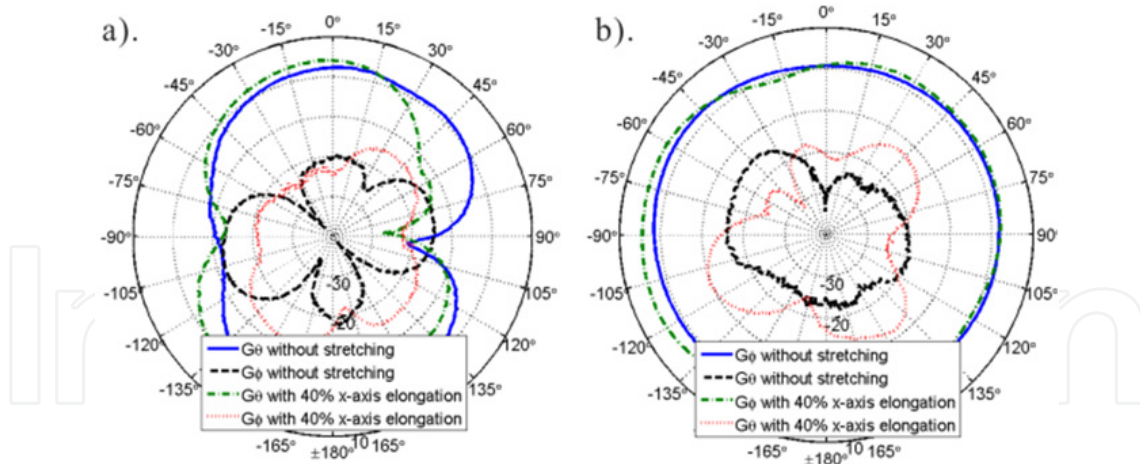
Figure 11. Measured a). *xz*- and b). *yz*-plane (according to the coordinate system in Fig. 7) radiation patterns at 2.5 GHz of the non-stretched and stretched antenna with 40% *x*-axis elongation.

Figure 12. Measured a). *xz*- and b). *yz*-plane (according to the coordinate system in Fig. 7) radiation patterns at 2.5 GHz of the non-stretched and stretched antenna with 40% *y*-axis elongation.
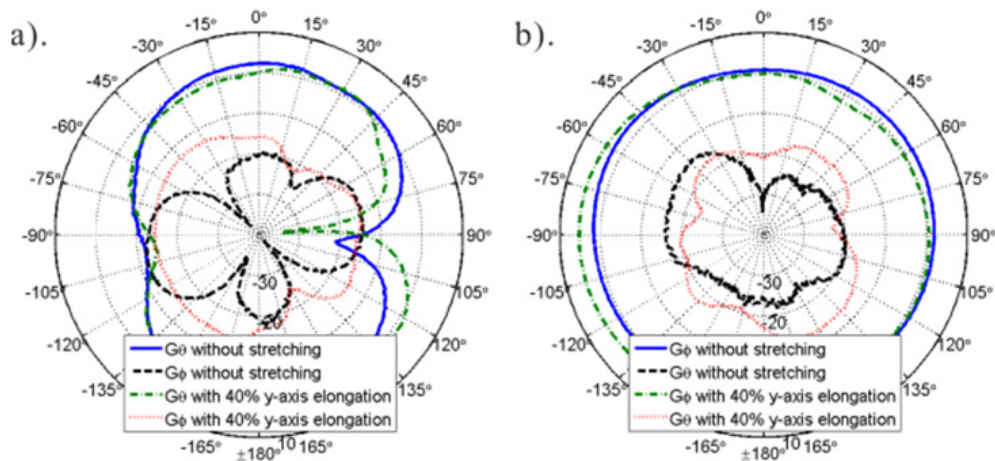
The measured radiation efficiency within the frequency range of 3-10 GHz is shown in Fig. 13. Although the radiation efficiency at the lower end of the frequency range decreases when the antenna is stretched, it is still greater than 70%. This, together with the experimental data on port impedance, indicates that the PICA prototype achieves good total antenna efficiency regardless of stretching.

Much work however remains. First of all, comprehensive environmental reliability and durability tests, e.g. vibration, temperature cycling, and aging, are needed, since it is indeed a new way of fabricating antennas, with new materials. Electrical characteristics of the antenna at extreme temperature condition, e.g. below the melting point of the liquid alloy, should be evaluated when a special measurement setup is established. Studies on antenna radio interfaces are also necessary. Development of fully integrated stretchable wireless electronic systems consisting of flexible thin embedded active chips, stretchable interconnects, and highly efficient stretchable antennas are the end objective, with a need for much research efforts.
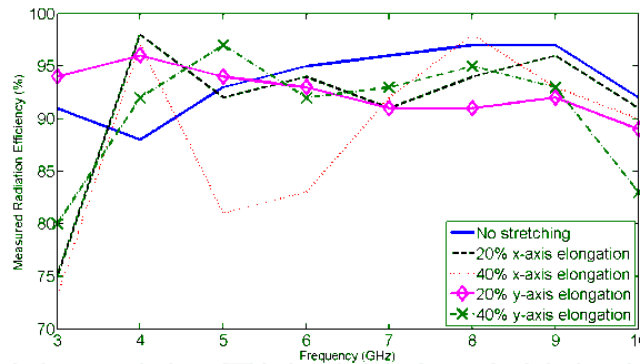
Figure 13. Experimental results on the radiation efficiency of the relaxed and flexed antennas.

5. Single-layer stretchable elastomeric integrated active RF electronics

The concept of microfluidics based passive stretchable elastomeric electronics has been further developed to the integrated device level utilizing localized stiff cells (LSCs), as illustrated in Fig. 14 [28]. A microfluidic, elastic, large-area antenna is realized in the same manner as the previous stretchable antennas, by incorporating liquid alloy into microstructured elastomeric channels. Established IC chips associated with passive components are assembled on small flexible laminates. Subsequently, a few tin-plated contact pins resembling cantilevers are soldered to the flexible circuits, and a semi-spherical solder ball is then mounted on the bottom surface of each contact pin on the other end to improve galvanic connection to the liquid fluid, *cf.* Fig. 14.e. Whereafter, the flexible circuits are embedded into the antenna substrate, with each contact pin immersing in the liquid alloy. In the end, uncured PDMS mixture droplets are deposited on top of the flexible circuits to locally enhance the stiffness of the elastomeric substrate and encapsulate the flexible circuits as well as the flex-to-stretch interfaces. The LSCs with enhanced stiffness than surrounding areas ensures that nearly zero stress and displacement between the rigid and the elastic structures would arise inside the LSCs when applying strains to the heterogeneously integrated device. The overall elasticity of the hybrid device is degraded compared to the standalone stretchable antennas due to the presence of the LSCs. But the reliability of the integrated device is greatly improved. Also, good wetting of the liquid metal alloy on tin-plated pins and solder balls ensures reliable electrical connections between contact pins and the antenna.

The proposed hybrid integration strategy was employed to implement a 900 MHz microfluidic stretchable RF radiation sensor, as seen in Fig. 15. The resulting sensor prototype is capable of performing real-time monitoring on the human exposure level to electromagnetic fields (EMF). Once the exposure level to EMFs exceeds the threshold power, the integrated light emission diode (LED) will be switched on. This sensor is of importance to human health as more and more EMFs are generated by today's telecom networks and mobile terminals, and might cause health issues. The integrated radiation sensor contains three sub-modules fully encased in a large-area elastomeric substrate, including a stretchable unbalanced loop antenna for capturing RF radiation from ambient environments, an RF power detection unit for converting received RF energy to the corresponding DC voltages, and a LED indicator for visualizing.
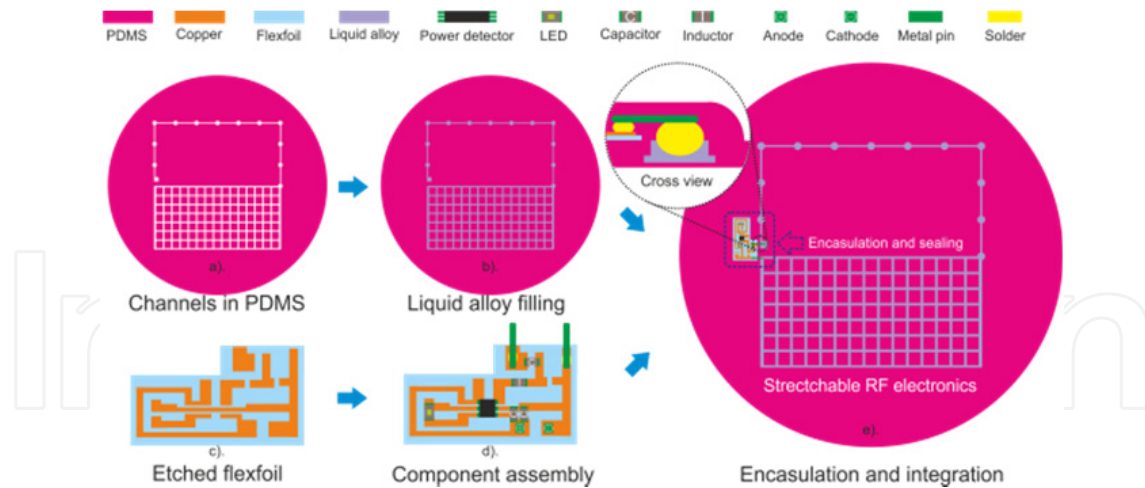
Figure 14. Schematic of the hybrid integration of the single-layer stretchable elastomeric RF electronics.
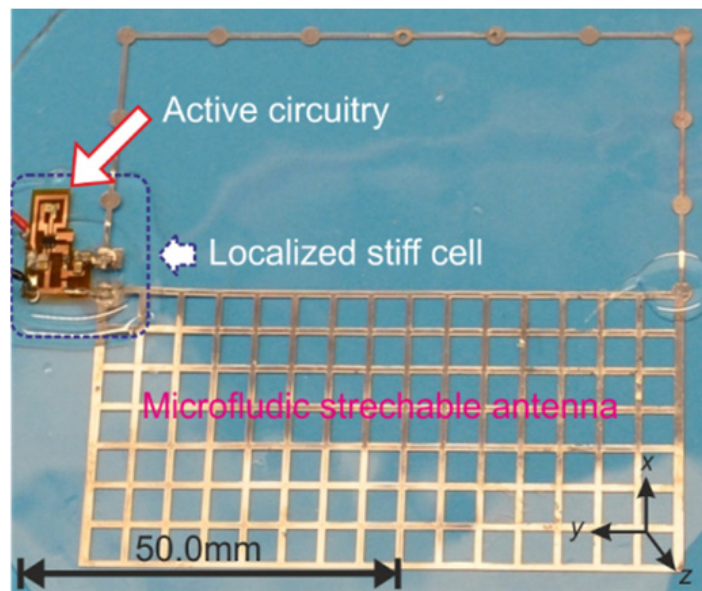

Figure 15. Photograph of the stretchable elastomeric RF radiation sensor prototype.

Prior to the hybrid integration, experimental evaluations on electrical characteristics of the standalone antenna and the RF power detection sub-module assembled on a flex foil are conducted. The implemented stretchable fluidic antenna exhibits similar mechanical and electrical performance as the previously presented unbalanced loop, but operates at a lower frequency of approximately 900 MHz. The power conversion sub-module in the integrated RF radiation sensor involves an off-the-shelf power detector IC chipset (Linear Technology, LT 5534), two decoupling and one coupling capacitors, an inductor for impedance matching at the RF input, and a green LED indicator, all assembled on a small flex foil with a size of 10 mm × 18 mm, as seen in Fig. 15. When the input RF energy at the detector exceeds the threshold power of the integrated device, the LED indicator is switched on, and vice versa. The entire integrated power detection unit can be powered by four serially connected AA rechargeable batteries with a DC supply voltage of 5.23 V. The power conversion behavior of the integrated device is first characterized using a signal generator and a digital

multimeter. Fig. 16 presents the measured DC voltages at the output of the power detection unit in response to varying input RF power at 900 MHz. A dynamic range of -60 dBm to 0 dBm can be achieved, and the threshold power for turning on/off the LED indicator is found to be slightly higher than -30 dBm.
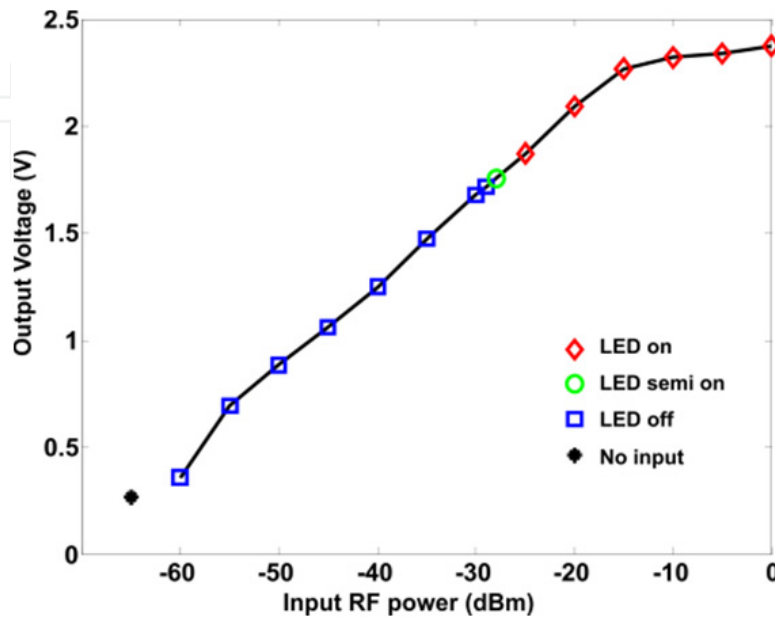

Figure 16. Measured output DC voltages of the RF power detection sub-module and the LED on/off states versus varying input RF power.

The integrated elastic radiation sensor device is tested in a demonstration setup in Fig. 17. The RF radiation source consists of an RF signal generator and a horn antenna placed 5 m away from the sensor device in the line-of-sight.
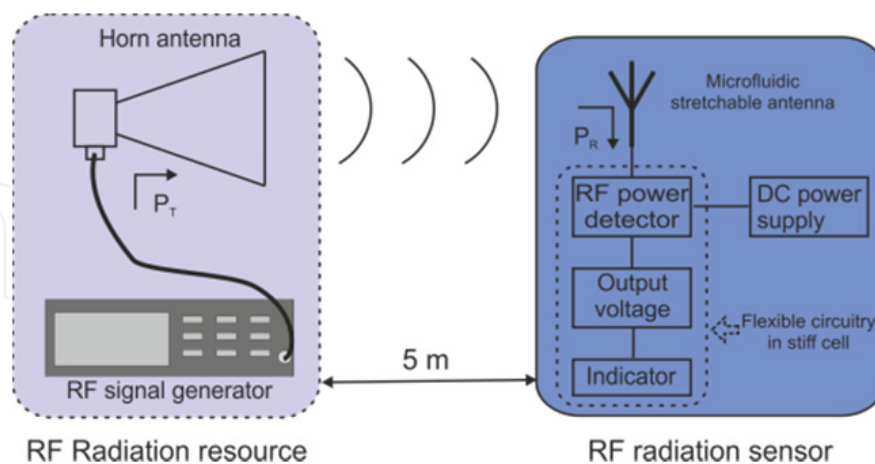

Figure 17. Schematic illustration of the RF radiation sensing demonstration setup.

Experiments presented in Fig. 18 verify that the resulting microfluidics based elastomeric integrated device maintains its radiation sensing capabilities even if it is strained along multiple axis. Extreme levels of twisting do not cause any failures in its operation either.
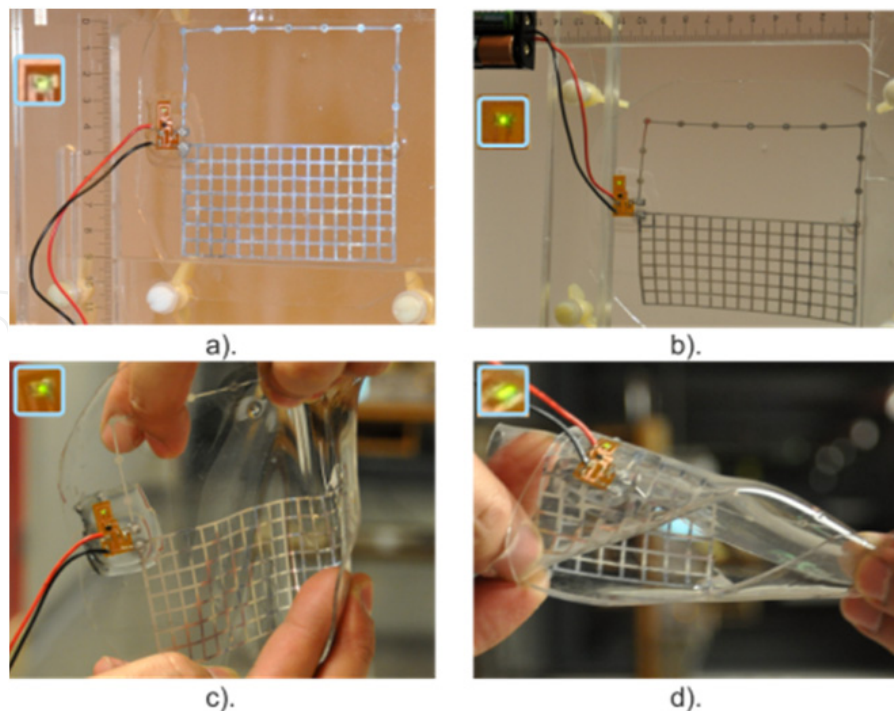
Figure 18. Photographs of the elastomeric RF radiation sensor device operating in ordinary office environment: a). relaxed state, b). with 15% strain applied along *y*-axis, e). with manually applied strain along multiple directions, and f). with severe twisting. The sensor was directly illuminated by a radiation source 5 m away. The coordinate system is shown in Fig. 15.

6. Multi-layer stretchable elastomeric integrated active RF electronics

Very recently, the emerging field of microfluidics based elastomeric electronics has been further advanced to multi-layer µFSRFEs, with the demonstration of a microfluidic, reversibly stretchable, large-area wireless strain sensor [29]. The manufacturing process for multi-layer elastomeric passive components resembles the single-layer fabrication, but with a few minor modifications and process steps added, *cf*. Fig. 19.

In summary, the upper and lower microfluidic channels are respectively constructed in the top and the bottom PDMS sheets, using standard soft lithography techniques. Then a few inlets and outlets are punched. In addition, the blank middle PDMS slab is prepared. The microstructured top elastomer layer is bonded to the blank silicone rubber slab using plasma boning, and addition inlets are punched on the bonded PDMS sheet. The bottom elastomer substrate is bonded to the previously bonded PDMS layers afterwards, using corona discharging activation. Prior to filling the upper microfluidic channels with galinstan fluid metal, the inlet 3 is sealed with a piece of Scotch® tape. Later, the ventilation outlets in the top silicone rubber sheet are encapsulated using PDMS prepolymer. Whereafter, both in the inlets 1 and 3 are taped, and galinstan alloy is injected into the lower microfluidic channels from the bottom side. All remaining ventilation outlets and the inlet 2 are then encapsulated, and the inlets 1 and 3 are reserved for connecting active circuitry in a heterogeneously integrated device.

Figure 19. Fabrication process of a multi-layer microfluidics based stretchable elastomeric passive electronic device.

The subsequent fabrication process steps are active circuit assembly and hybrid device integration, which resemble the manufacturing and the integrated processes presented in the previous section. Schematic illustrations describing the entire assembly and integration procedure are displayed in Fig. 20, and not discussed in detail in this section.
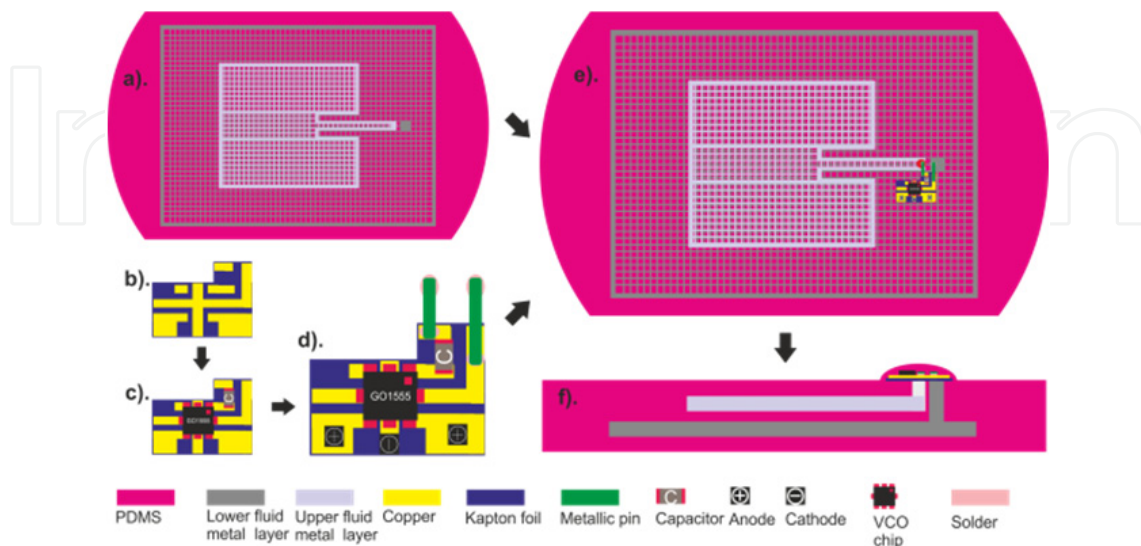

Figure 20. Schematic drawings of the integration procedure for a multi-layer stretchable, microfluidic integrated electronic device.

The first resulting integrated device based on multi-layer μFSRFEs is a self-contained wireless strain sensor, fully encased in a thin large-area silicone elastomer, as shown in Fig. 21. A stretchable liquid metal microstrip patch antenna comprising an upper rectangular meshed patch and a lower ground plane constructed in the same manner, takes up the major area of the hybrid device. It is worthy mentioning that this antenna not only serves as a radiator like any other conventional antennas, but also acts as a sensing device owing to its varying electrical characteristics in response to mechanical deformation. The entire integrated sensor device is slightly larger than its meshed fluid metal ground with a size of 100 mm × 80 mm, and approximately four times as big as the antenna patch. Though the liquid metal patch is the actual strain sensing element, the large ground plane can also serve an effective sensing area, and extend the strain sensing functionality to almost the entire device. Apart from the self-contained wireless strain sensor, a custom-designed personal computer (PC)-assisted radio receiver for remotely collecting, processing, and storing the measured data wirelessly transmitted from the integrated sensor device is also implemented. It removes the need for costly RF measurement facilities, and significantly reduces the cost for building up a complete system.
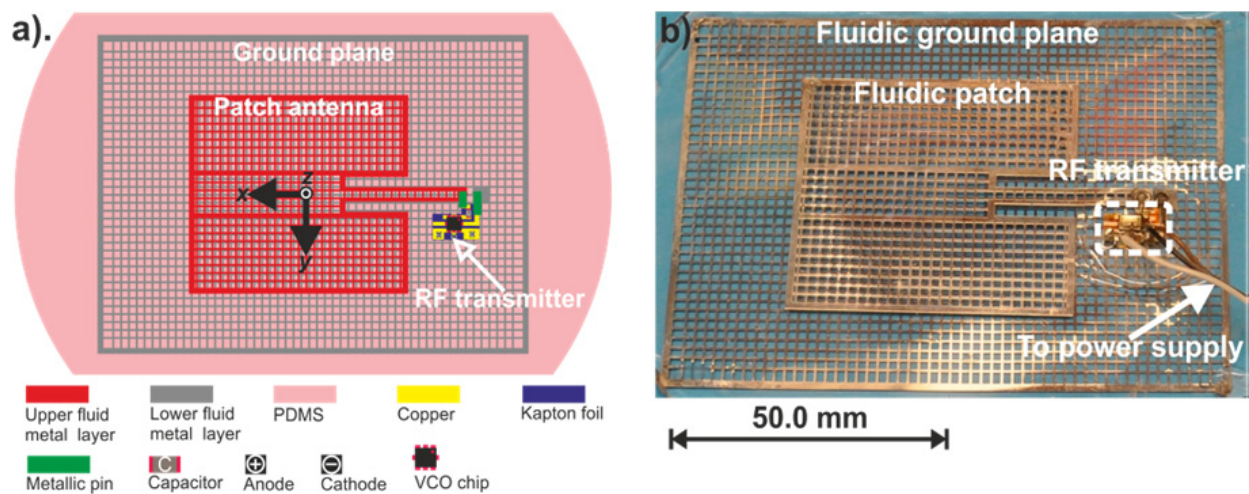

Figure 21. Demonstrated microfluidic reversibly stretchable wireless strain sensor: a). schematic illustration, and b). optical photograph of the resulting device.

Port impedance and radiation characteristics of the standalone, mechanically reconfigurable, elastomeric patch antenna in its relaxed and flexed states are measured. Excellent port impedance matching around 1.46 GHz along with very good correlation between the simulated and measured reflection coefficients of the non-stretched antenna are seen in Fig. 22.a. Applying increasing strain of up to 15% along its x-axis introduces persistent downshift of its resonant frequency of the patch antenna. The lowest resonant frequency of approximately 1.33 GHz is achieved at the maximum x-axis elongation of 15%.The measured resonant frequency of the relaxed antenna is slightly less than the minimum operational frequency of the integrated transmitter circuit. This negative offset is crucial to strain sensing, since persistently rising antenna mismatch losses at the operational frequencies in response to increasing stressing along the x-axis of the hybrid device.

Furthermore, this frequency offset should be as little as possible to avoid too high mismatch losses so that reasonably long remote sensing ranges as well as sufficient sensing sensitivity can be attained. Placing the antenna original resonant frequency above the highest operational frequency of the transmitter is not an option, as inconsistent variations of mismatch losses would occur if the antenna based strain sensor is stressed from its relaxed state to a high tensile strain.

Measured radiation patterns, including mismatch losses, at 1.46 GHz, of the relaxed and flexed antennas are shown in Figs. 22.b and c. The realized peak gain is measured along the +z-axis (according to the coordinate system depicted in Fig. 21.a.) of the mechanically reconfigurable antenna, and greatly degraded from 2.0 dBi to -10.7 dBi while applying an increasing strain from 0% to 15% along its x-axis. The meshed ground plane directs the radiation forward, with a front-to-back ratio as high as 10.0 dB, regardless of stretching. Moreover, the cross-polarization discrimination is very good in both relaxed and strained cases.
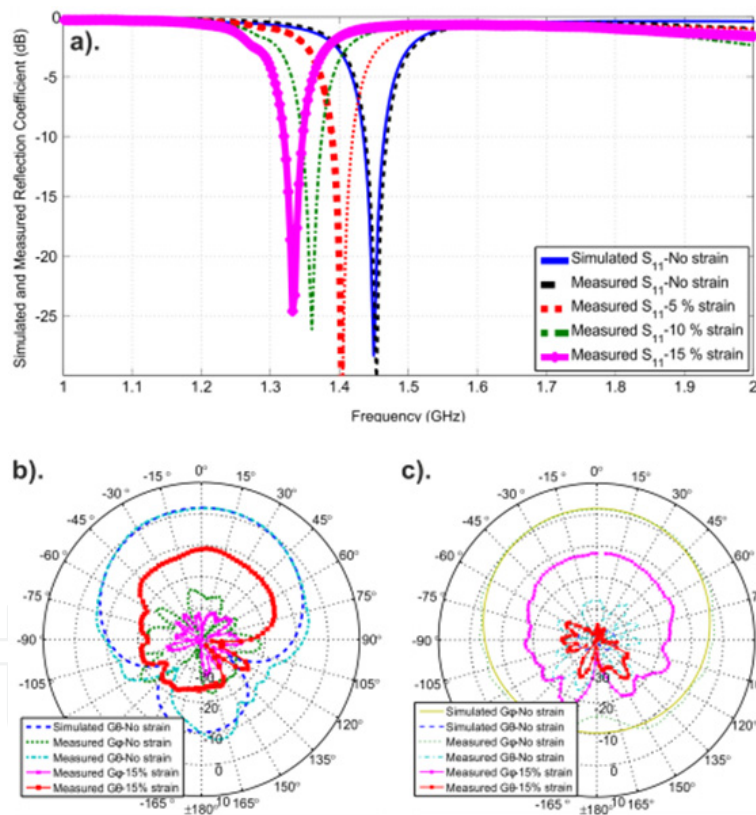

Figure 22. a). Simulated and measured reflection coefficients of the elastomeric fluid metal patch antenna in its relaxed state, and with different strains along the x-axis (according to the coordinate system in Fig. 21). b). xz- and c). yz-plane radiation patterns (including mismatch losses) at the original resonant frequency of the elastic antenna in its relaxed state, and with 15% elongation along its x-axis. The antenna gain along ϕ and θ orientations is defined as G_ϕ and G_θ, respectively. The antenna co- and cross-polarization along +z-axis are in parallel to the x- and y-axis.

Mechanical properties of the elastomeric patch antenna are evaluated after characterizations on its electrical performance. The implemented antenna prototype is more than twice as

thick as the previously demonstrated stretchable RF electronic devices, and thus features degraded mechanical deformability. Yet moderate twisting or folding do not cause any mechanical damages to the fluidic patch antenna during experiments.

The measured total efficiency of the standalone stretchable patch antenna including mismatch losses is 36.9% in its relaxed state at 1.46 GHz. Straining the patch to 15% along its x-axis leads to considerable total efficiency drop of 33.8%. In the intermediate states with the strains between 5% and 10%, the total efficiency of 11.5% and 5.8% is achieved according to the experiments.

The system demonstration setup is first calibrated by characterizing the output DC voltages of the RF power detector with different static stresses applied to the integrated wireless strain sensor, as presented in Fig. 23. A fairly linear decline of the measured DC voltages versus increasing mechanical elongation along the x-axis of the self-contained sensor device is seen, and can be explained by decreased resonant frequencies and increased mismatch losses of the transmitting, elastomeric antenna as a result of incremental stretching. As co-polarization components dominate in both microfluidic stretchable patch antenna in the hybrid sensor and the receiving horn in the custom-designed RF receiver, the measured output voltages with respect to the cross-polarization are considerably lower than that of the co-polarization, and also exhibit smaller variations versus different strains. The steepest voltage decline in response to increasing stretch is found in the case of the co-polarization measured in an anechoic chamber. When it comes to ordinary office environment, the presence of reflections and scatterings limits the range of voltage variations.
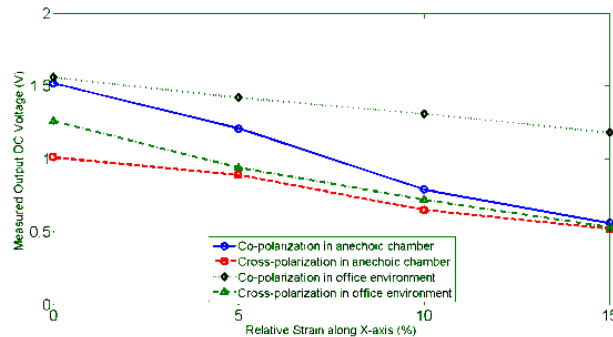

Figure 23. Measured output DC voltages at the receiver versus varying mechanical stress along the x-axis (according to the coordinate system in Fig. 21) applied to the integrated strain sensor. Its co- and cross-polarizations along the +z-axis were in parallel to the x- and y-axis, and the receiving standard horn was horizontally polarized.

Fig. 24 shows the demonstration of remote sensing of repeated body motion in a corridor of ordinary office environment, using the resulting wireless strain sensor prototype. Periodically repeated dynamic strains of up to 15% along its x-axis, with a period of 10s and a duty cycle of 50%, are manually applied to the two shorter edges of the integrated, elastic, strain sensor. The output DC voltages in the PC-assisted RF receiver varying with mechanical strains of the integrated, body-worn, sensor device, are continuously monitored and recorded, *cf.* Fig. 24.c. The measured data of six cycles, well correlating with the applied varying tensile strains, are presented in the subplot in Fig. 24.c, in which six fairly uniform,

quasi-rectangular waves with varying amplitude between 1.28V and 1.55V are recorded in an overall period of 60s. This experimental data also verifies that the implemented wireless strain sensor can rapidly return to its relaxed state without any hysteresis, once removing the applied stress. This great feature reflects reversible deformability as well as high degree of elasticity of the multi-layer µFSRFEs based sensor device.
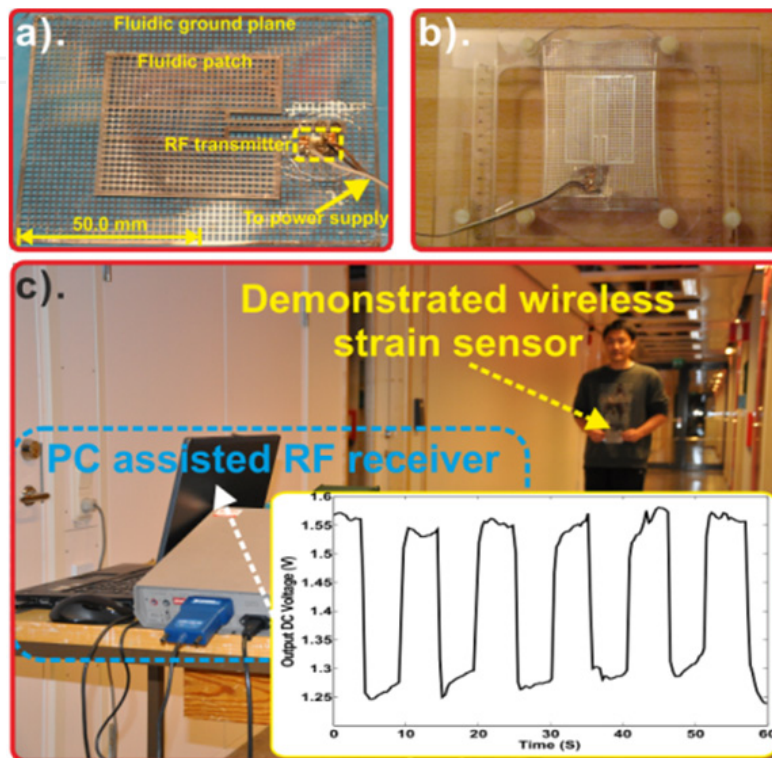

Figure 24. Integrated elastomeric strain sensor a). in its original state and b). with 15% vertical strain. c). system demonstration (periodical manual straining). Real-time recorded data at the PC-assisted RF receiver 5m away is presented in the subplot.

7. Conclusion

Recent advances in the emerging field of elastomeric electronics that are able to be conformed into complex curvilinear shapes, or be compressed, twisted, and stressed to extreme degrees, have been briefly reviewed. Various techniques and strategies for realizing bendable, flexible, stretchable elastomeric electronic devices and system have been discussed. As the main focus, elastomeric electronics based on microfluidic approaches have been addressed in detail. Fabrication processes, hybrid integration techniques, as well as appealing application examples involving single- and multi-layer µFSRFEs have also been presented.

Microfluidics based elastic electronics together with other members in the family of elastomeric electronics are introducing a revolution to the world of electronics, and shaping the future for electronics so as to change our tomorrow's daily life and contribute to our networked society. It is anticipated that more than 50 billion devices will be wirelessly connected by 2020, which would involve units as intelligent as smartphones/tablets, and as soft as elastomeric electronics.

Acknowledgement

Author details

Shi Cheng
Ericsson AB, Stockholm, Sweden

8. References

[1] Bowden N, Brittain S, Evans AG, Hutchinson JW, Whitesides GM (1998) Spontaneous Formation of Ordered Structures in Thin Films of Metals Supported on an Elastomeric Polymer. Nature 393: 146-149.

[2] Watanabe M, Shirai H, Hirai T (2002) Wrinkled Polypyrrole Electrode for Electroactive Polymer Actuators. J. Appl. Phys. 92: 4631.

[3] Lacour SP, Wagner S, Huang ZY, Suo ZG (2003) Stretchable Gold Conductors on Elastomeric Substrates. Appl. Phys. Lett. 82: 2404.

[4] Lacour SP, Jones J, Wagner S, Li T, Suo ZG (2005) Stretchable Interconnects for Elastic Electronic Surfaces. Proc. IEEE 93: 1459-1467.

[5] Kim DH, Ahn JH, Choi WM, Kim HS, Kim TH, Song JZ, Huang Y, Liu ZJ, Lu C, Rogers JA (2008) Stretchable and Foldable Silicon Integrated Circuits. Science 320: 507-511.

[6] Kim DH, Song JZ, Choi WM, Kim HS, Kim RH, Liu ZJ, Huang Y, Hwang KC, Zhang YW, Rogers JA (2008) Materials and Noncoplanar Mesh Designs for Integrated Circuits With Linear Elastic Responses to Extreme Mechanical Deformations. Proc. Nat. Acad. Sci. USA 105: 18675-18680.

[7] Ko HC, Stoykovich MP, Song J, Malyarchuk JV, Choi WM, Yu CJ, Geddes JB, Xiao J, Wang S, Huang Y, Rogers JA (2008) A Hemispherical Electronic Eye Camera Based on Compressible Silicon Optoelectronics. Nature 454: 748-753.

[8] Kim DH, Kim YS, Wu J, Liu Z, Song J, Kim HS, Huang Y, Hwang KC, Rogers JA (2009) Ultrathin Silicon Circuits With Strain-Isolation Layers and Mesh Layouts for High-Performance Electronics on Fabric, Vinyl, Leather, and Paper. Adv. Mater. 21: 3703–3707.

[9] Kim DH, Lu N, Ghaffari R, Kim YS, Lee SP, Xu L, Wu J, Kim RH, Song J, Liu Z, Viventi J, de Graff B, Elolampi B, Mansour M, Slepian MJ, Hwang S, Moss JD, Won SM, Huang Y, Litt B, Rogers JA (2011) Materials for Multifunctional Balloon Catheters With Capabilities in Cardiac Electrophysiological Mapping and Ablation Therapy. Nat. Mater. 10: 316-323.

[10] Kim DH, Lu N, Ma R, Kim YS, Kim RH, Wang S, Wu J, Won SM, Tao H, Islam A, Yu KJ, Kim TI, Chowdhury R, Ying M, Xu L, Li M, Chung HJ, Keum H, McCormick M, Liu P,VZhang YW, Omenetto FG, Huang Y, Coleman T, Rogers JA (2011) Epidermal Electronics Science 333: 838-843.

[11] Baca AJ, Meitl MA, Ko HC, Mack S, Kim HS, Dong J, Ferreira PM, Rogers JA (2007) Printable Single-Crystal Silicon Micro/Nanoscale Ribbons, Platelets and Bars Generated from Bulk Wafers. Adv. Func. Mater. 17: 3051–3062.

[12] Mack S, Meitl MA, Baca AJ, Zhu ZT, Rogers JA (2006) Mechanically Flexible Thin-Film Transistors That Use Ultrathin Ribbons of Silicon Derived from Bulk Wafers. Appl. Phys. Lett. 88: 213101.

[13] Brosteaux D, Axisa F, Gonzalez M, Vanfleteren J (2007) Design and Fabrication of Elastic Interconnections for Stretchable Electronic Circuits. IEEE Electron Device Lett. 28: 552-524.

[14] Huyghe B, Rogier H, Vanfleteren J, Axisa F (2008) Design and Manufacturing of Stretchable High-Frequency Interconnects. IEEE Trans. Adv. Packaging. 31: 802-808.

[15] Carta R, Jouranda P, Hermansa B, Thonéa J, Brosteauxb D, Vervustb T, Bossuytb F, Axisab F, Vanfleteren J, Puersa R (2009) Design and Implementation of Advanced Systems in A Flexible-Stretchable Technology for Biomedical Applications. Sensors Actuat. A-Phys. 156: 79-87.

[16] Niu X, Peng S, Liu L, Wen W, Sheng P (2007) Characterizing and Patterning of PDMS-Based Conducting Composites. Adv. Mater. 19: 2682.

[17] Sekitani T, Noguchi Y, Hata K, Fukushima T, Aida T, Someya T (2008) A Rubberlike Stretchable Active Matrix Using Elastic Conductors. Science 321: 1468-1472.

[18] Siegel AC, Shevkoplyas SS, Weibel DB, Bruzewicz DA, Martinez AW, Whitesides GM (2006) Cofabrication of Electromagnets and Microfluidic Systems in Poly(dimethylsiloxane). Angew. Chem. Int. Edit. 45: 6877-6882.

[19] Siegel AC, Bruzewicz DA, Weibel DB, Whitesides GM (2007) Microsolidics: Fabrication of Three-Dimensional Metallic Microstructures in Poly(dimethylsiloxane). Adv. Mater. 19: 727-733.

[20] Hu H, Shaikh K, Liu C (2007) Super Flexible Sensor Skin Using Liquid Metal As Interconnect. Proceeding of IEEE Sensors 1:815-817.

[21] Kim HJ, Son C, Ziaie B (2008) A Multiaxial Stretchable Interconnect Using Liquid-Alloy-Filled Elastomeric Microchannels. Appl. Phys. Lett. 92: 011904.

[22] Kim HJ, Maleki T, Wei P, Ziaie B (2009) A Biaxial Stretchable Interconnect With Liquid-Alloy-Covered Joints on Elastomeric Substrate. J. Microelectromech. S. 18: 138-146.

[23] Cheng S, Rydberg A, Hjort K, Wu ZG (2009) Liquid Metal Stretchable Unbalanced Loop Antenna. Appl. Phys. Lett. 94: 144103.

[24] Cheng S, Wu ZG, Hallbjörner P, Hjort K, Rydberg A (2009) Foldable and Stretchable Liquid Metal Planar Inverted Cone Antenna. IEEE Trans. Antennas Propag. 57: 3765–3771.

[25] So JH, Thelen J, Qusba A, Hayes GJ, Lazzi G, Dickey MD (2009) Reversibly Deformable and Mechanically Tunable Fluidic Antennas. Adv. Func. Mater. 19: 3632-3637.

[26] Kubo M, Li X, Kim C, Hashimoto M, Wiley BJ, Ham D, Whitesides GM (2010) Stretchable Microfluidic Radiofrequency Antennas. Adv Mater. 22: 2749 - 2752.

[27] Khan MR, Hayes GJ, So JH, Lazzi G, Dickey MD (2011) A Frequency Shifting Liquid Metal Antenna With Pressure Responsiveness. Appl. Phys. Lett. 99: 013501.

[28] Cheng S, Wu ZG (2010) Microfluidic Stretchable RF Electronics. Lab Chip 10: 3227 - 3234.

[29] Cheng S, Wu ZG (2011) A Microfluidic, Reversibly Stretchable, Large-Area Wireless Strain Sensor. Adv. Func. Mater. 21: 2282-2290.